

# Atomic inner-shell X-ray laser at 1.46 nanometres pumped by an X-ray free-electron laser

Nina Rohringer<sup>1†</sup>, Duncan Ryan<sup>2</sup>, Richard A. London<sup>1</sup>, Michael Purvis<sup>2</sup>, Felicie Albert<sup>1</sup>, James Dunn<sup>1</sup>, John D. Bozek<sup>3</sup>, Christoph Bostedt<sup>3</sup>, Alexander Graf<sup>1</sup>, Randal Hill<sup>1</sup>, Stefan P. Hau-Riege<sup>1</sup> & Jorge J. Rocca<sup>2</sup>

Since the invention of the laser more than 50 years ago, scientists have striven to achieve amplification on atomic transitions of increasingly shorter wavelength<sup>1–7</sup>. The introduction of X-ray free-electron lasers<sup>8–10</sup> makes it possible to pump new atomic X-ray lasers<sup>11–13</sup> with ultrashort pulse duration, extreme spectral brightness and full temporal coherence. Here we describe the implementation of an X-ray laser in the kiloelectronvolt energy regime, based on atomic population inversion and driven by rapid K-shell photo-ionization using pulses from an X-ray free-electron laser. We established a population inversion of the K $\alpha$  transition in singly ionized neon<sup>14</sup> at 1.46 nanometres (corresponding to a photon energy of 849 electronvolts) in an elongated plasma column created by irradiation of a gas medium. We observed strong amplified spontaneous emission from the end of the excited plasma. This resulted in femtosecond-duration, high-intensity X-ray pulses of much shorter wavelength and greater brilliance than achieved with previous atomic X-ray lasers. Moreover, this scheme provides greatly increased wavelength stability, monochromaticity and improved temporal coherence by comparison with present-day X-ray free-electron lasers. The atomic X-ray lasers realized here can be useful for high-resolution spectroscopy and nonlinear X-ray studies.

The emergence of short-wavelength X-ray free-electron lasers<sup>8–10</sup> (XFELs), delivering femtosecond X-ray pulses that exceed the peak brilliance of synchrotron sources by many orders of magnitude, has potential to open a pathway to studying nonlinear interactions of X-rays with matter<sup>15–21</sup>. Especially appealing are ideas of transferring nonlinear spectroscopic techniques to the X-ray regime, to study photoinduced charge transfer, nuclear dynamics, chemical reactions, valence wavepacket propagation in molecules or phase transitions in solids at high temporal and spatial resolution. Nonlinear techniques to study these effects, such as X-ray stimulated coherent Raman spectroscopy<sup>19,20</sup> or four-wave mixing<sup>18,21</sup>, would, however, require ultrashort (preferably subfemtosecond), temporally coherent, synchronized two-colour X-ray sources. Present-day XFELs are based on self-amplified spontaneous emission (SASE) and start from noise. Although they are of unprecedented brightness, the pulses of SASE free-electron lasers have a fluctuating spectrum and limited temporal coherence<sup>22</sup>. A way to improve SASE pulses and to create a synchronized two-colour source in the X-ray regime is to use a SASE pulse to pump an atomic X-ray laser (XRL)<sup>11–13</sup>.

Soft-X-ray lasers were first realized in 1984 at wavelengths near 20 nm (refs 2,3). In the soft-X-ray/vacuum-ultraviolet regime, population inversion is typically achieved by collisional excitation or recombination into excited states of highly ionized atoms in a hot, dense plasma<sup>4–7</sup>. The first XRL in the kiloelectronvolt regime was proposed in 1967 and is based on establishing a population inversion by rapid photo-ionization of an inner-shell electron<sup>1</sup>. In 1983 this scheme was demonstrated at optical wavelengths<sup>23</sup>, and a few years later a

similar scheme was demonstrated in the vacuum ultraviolet using Auger-decay pumping following inner-shell photo-ionization<sup>24</sup>. The photo-ionization scheme was extensively studied in theory for different gain materials and pump sources in the X-ray regime<sup>14,25–27</sup>. Notably, detailed calculations for the neon K $\alpha$  transition pumped by laser-produced plasma X-rays were presented in 1991<sup>14</sup>. However, the lack of sufficiently fast and intense X-ray sources has so far precluded the realization of the photo-ionization scheme in the X-ray regime. More recently, calculations for neon pumped by XFEL radiation, which served as the design basis for this experiment, have been presented<sup>13</sup>.

When irradiated by X-rays slightly higher in energy than the ionization edge of an inner electronic shell, photo-ionization of an atom proceeds from the inside out, creating short-lived core-excited ions, which subsequently relax by means of Auger or radiative decay. At intensities achievable with XFELs, inner-shell photo-ionization happens on a timescale comparable to the lifetime of core-excited states, so that states of high ionic charge can be reached within a few femtoseconds and double-core-excited ‘hollow’ ions can be created<sup>28</sup>. Moreover, rapid photo-ionization results in short-lived population inversions, which can be exploited for lasing from the valence to the core level.

In our experiment, which was carried out at the Linac Coherent Light Source<sup>8</sup> (LCLS) of the SLAC National Accelerator Laboratory, XFEL pulses of 960-eV photon energy were focused into a volume of neon gas at  $\sim 500$  torr to spot sizes of 1–2- $\mu\text{m}$  radius, to create a long, narrow column of transiently core-excited ions (Fig. 1). XFEL pulse energies on target were between 0.02 and 0.27 mJ, and the pulse duration was 40–80 fs. This resulted in intensities up to  $2 \times 10^{17} \text{ W cm}^{-2}$  and an inverse photo-ionization rate of  $\sim 4$  fs, which is comparable to the Auger lifetime of the 1s core hole, namely 2.4 fs. Although the decay of the core-excited state is dominated by the Auger process, there is a small probability (1.8%) that the ion will undergo a spontaneous radiative decay, emitting a photon with an energy of 849 eV. Photons that are spontaneously emitted near the front end of the plasma column generate exponentially amplified stimulated emission along the direction of the XFEL pulse, which prepares atoms in the excited state, just as the atomic line radiation from previously excited atoms reaches them. In traditional plasma-based XRLs, the width of the transition is determined by Doppler, lifetime and collisional broadening. In the present scheme, the density is low and the plasma remains cold, with the result that the transition is mainly lifetime-broadened by Auger decay. The line profile of the spontaneous emission before strong amplification by stimulated emission is therefore Lorentzian with a width of 0.27 eV.

A grazing-incidence grating spectrometer with a CCD detector was used to monitor the spectrum of the transmitted XFEL pump source and the atomic XRL radiation. The raw single-shot image shown in Fig. 1b provides strong evidence of lasing. The relatively broad line (Fig. 1b, bottom) is the transmitted XFEL pulse. The narrow atomic line radiation is visible at 849 eV, with peak intensities one order of

<sup>1</sup>Lawrence Livermore National Laboratory, 7000 East Avenue, Livermore, California 94551, USA. <sup>2</sup>Colorado State University and NSF Engineering Research Center for Extreme Ultraviolet Science and Technology, Fort Collins, Colorado 80523, USA. <sup>3</sup>LCLS, SLAC National Accelerator Laboratory, 2575 Sand Hill Road, Menlo Park, California 94025, USA. <sup>†</sup>Present address: Max Planck Advanced Study Group, Center for Free-Electron Laser Science, c/o DESY, Notkestrasse 85, 22607 Hamburg, Germany.

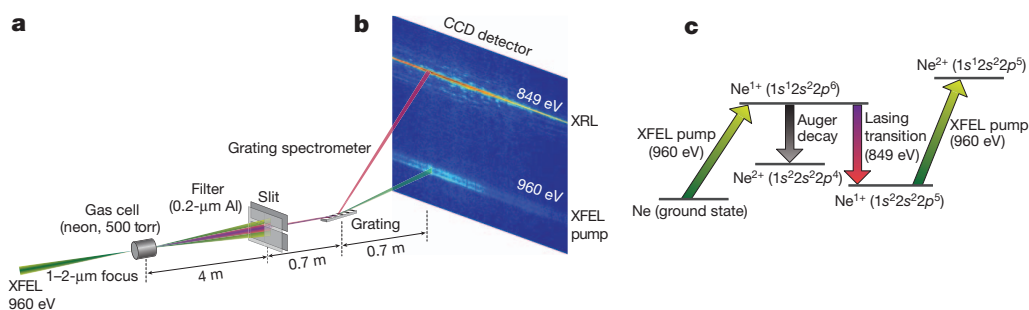


**Figure 1 | Experimental scheme.** **a**, The XFEL beam is focused into a gas cell filled with neon to a focus spot of radius 1–2  $\mu\text{m}$ . A flat-field X-ray grating spectrometer was positioned  $\sim 4$  m from the interaction region. **b**, The charge-coupled-device (CCD) image of the transmitted XFEL pump (bottom) and the XRL (top). **c**, Level scheme. Population inversion of the  $1s^1 2s^2 2p^6$ -to- $1s^2 2s^2 2p^5$

magnitude higher than that of the strongly attenuated XFEL. Fluorescence would result in  $\sim 50$  photons entering the spectrometer set-up, which is undetectable in the current configuration. Figure 2 shows line-outs of three different single-shot spectra for an XFEL energy of  $\sim 0.25$  mJ. By contrast with the broad (full-width at half-maximum (FWHM) of 8 eV) and jittering (FWHM of 14 eV) spectra of the XFEL pulses, the atomic line has a reproducible spectral shape with narrow width and fixed centroid. The measured FWHM, of 2 eV, is limited by the resolution of the spectrometer.

To demonstrate exponential amplification on the atomic line transition, we varied the incoming XFEL energy. To average over the large statistical fluctuations in the XRL output, we gathered a set of 950 spectral images in a series of ten-shot integrations. Figure 3 shows the averaged number of photons in the neon  $K\alpha$  line for each of the images as a function of the averaged pulse energy. Doubling the XFEL energy from 0.12 to 0.24 mJ results in an average increase in the XRL line energy by four orders of magnitude. The XRL pulse energy distribution is relatively broad at a given pump energy, reflecting the large shot-to-shot variation of the gain due to the stochastic properties of the SASE pulse. Also shown in Fig. 3 is a comparison to a one-dimensional, time-dependent, self-consistent gain model<sup>13</sup> (see also Supplementary Information). There is good agreement between the calculated and measured energies in the neon  $K\alpha$  line and in the transmitted XFEL pump (Supplementary Fig. 6).

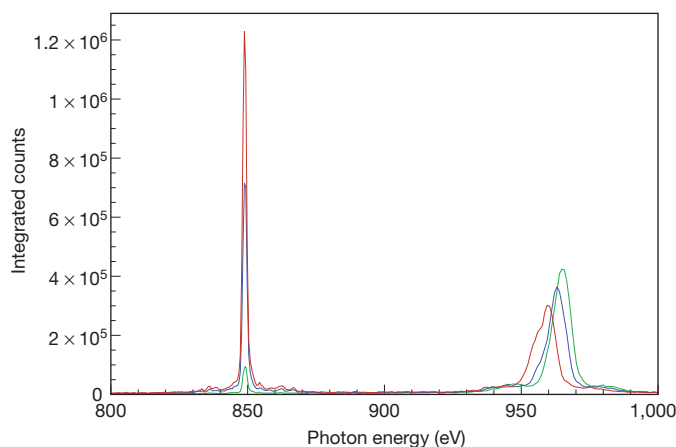


**Figure 2 | Single-shot spectra of the atomic XRL line and transmitted XFEL pump.** Horizontally integrated spectra for three shots with similar pulse energies, but slightly varying XFEL photon energies. The neon gas attenuates the XFEL and XRL lines by factors of  $2.5 \times 10^3$  and 2, respectively. The neon  $K\alpha$  line is centred at 849 eV and has a FWHM of 2 eV limited by instrument resolution. The neon  $K\alpha$  line shows satellite peaks on both sides of the main peak. Their intensities closely follow that of the main peak and are most probably ghost lines from the spectrometer grating.

transition is created by K-shell photo-ionization of neutral neon. The Auger decay time of the inverted state (2.4 fs) dominates the kinetics of the system in the small-signal-gain regime. The lower lasing state is depleted by K-shell photo-ionization.

To estimate the influence of the fluctuating temporal profiles of the XFEL on the gain, we calculated the small-signal gain coefficient for an ensemble of 1,000 numerically generated SASE pulses (Fig. 4). The gain for this self-terminating scheme is characterized by a rise time of 5 fs and a peak of  $64 \text{ cm}^{-1}$ . The gain duration has a FWHM of 20 fs and is determined by the convolution of the rate to deplete the neutral atoms with the exponential Auger decay. The variation in the peak gain due to the SASE pump is considerable; the standard deviation is 30%.

The traditional method of determining the gain-length product (GL) is by measuring the output energy versus length. We estimate GL by comparing the measured value of the output energy with a simple theoretical estimate (Supplementary Information). For the single shot with the highest XRL output,  $1.1 \pm 0.4 \mu\text{J}$ , we estimate that  $\text{GL} = 19.2\text{--}21.3$ , whereas for average shots with 0.24-mJ XFEL energy we deduce  $\text{GL} = 17\text{--}19.3$ . This is consistent with  $\text{GL} = 19$ , the result calculated using our one-dimensional model. Owing to strong absorption of the XFEL, the gain coefficient decreases as a function of propagation depth, with a calculated decay length of 0.28 cm. This is somewhat longer than the expected attenuation length in neutral neon, of 0.22 cm, owing to bleaching. Assuming a gain region 0.28 cm in length, we estimate an effective gain coefficient of  $61\text{--}70 \text{ cm}^{-1}$  at 0.24-mJ XFEL energy. Saturation of the exponential amplification cannot be discerned in the experimental data presented in Fig. 3. Our

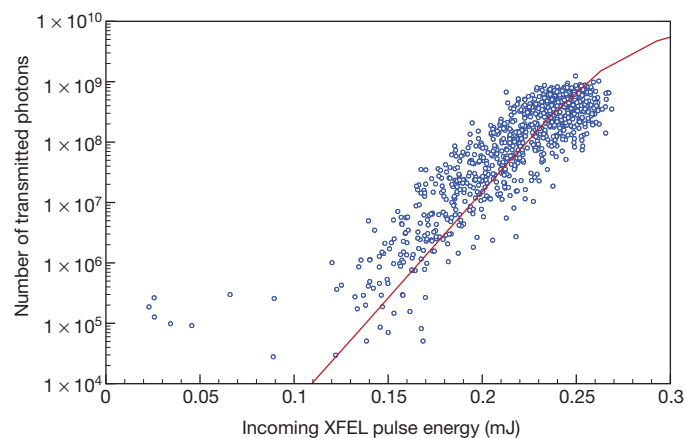


**Figure 3 | Dependence of the XRL output on pump power.** Average number of transmitted photons of the neon  $K\alpha$  line for ten consecutive XFEL shots, as a function of the average XFEL pulse energy on target (s.d.,  $\pm 0.014$  mJ). We assumed a beamline transmission of 18%. The determined number of  $K\alpha$  photons has an error of  $\sim 30\%$ . The small linear signal below a pulse energy of 0.15 mJ results from spectral tails of the XFEL reaching into the 849-eV energy region of the XRL line. Results of a one-dimensional model are shown in red, assuming a density of  $1.6 \times 10^{19} \text{ atoms cm}^{-3}$ , an interaction length of 1.8 cm, a pulse duration of 40 fs and a focal radius of 2  $\mu\text{m}$ .

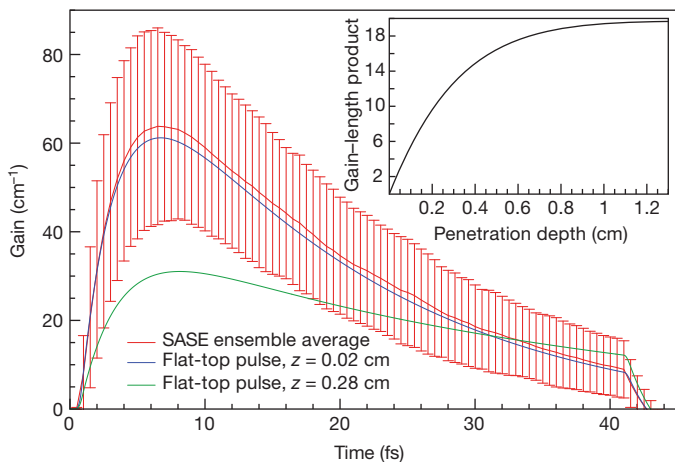


**Figure 4 | Simulation of the gain.** Temporal profile of the average gain (error bars, s.d.) at a density of  $1.6 \times 10^{19}$  atoms  $\text{cm}^{-3}$  for an ensemble of 1,000 SASE pulses of 40-fs pulse duration, an energy of 0.24 mJ and a coherence time of 0.3 fs. Also shown is the temporal profile of the gain as determined by the self-consistent gain calculations at penetration depths of  $z = 0.02$  cm (blue) and 0.28 cm (green) for a flat-top pulse with a 0.5-fs Gaussian ramp on. Inset, integrated gain-length product as a function of the penetration depth in the medium.

simulations, however, suggest that we are close to the onset of saturation, which according to our model is reached at  $GL = 22$ . In traditional XRLs, saturation sets in at far lower values, of  $GL \approx 15$  (ref. 5). In our scheme, the small angular divergence, the fast upper-state decay and the absence of refraction all contribute to the higher value of  $GL$  needed to reach saturation.

The measured output parameters of the neon XRL are a maximum single-shot energy of  $1.1 \pm 0.4 \mu\text{J}$  and an angular divergence of 1 mrad (see spatial beam intensity profile in Supplementary Fig. 5). This energy corresponds to  $\sim 8 \times 10^9$  photons in the neon  $K\alpha$  line and an energy conversion efficiency of  $4 \times 10^{-3}$ . The geometry of the gain medium (radius, 1–2  $\mu\text{m}$ ; length, 0.28 cm) results in a Fresnel number of  $\sim 1$ , such that the XRL is expected to be transversely coherent<sup>4</sup>. Our model predicts an average pulse duration of 5-fs FWHM. The XRL, a gain-swept amplifier characterized by a fast build-up of the population inversion and a short upper-state lifetime, is expected to be nearly transform limited and longitudinally coherent<sup>29</sup>. We estimate the spectral width to be 0.27 eV, resulting in a relative bandwidth of 0.03%, determined by Fourier transform of the square root of the temporal flux profile. To determine the spectral, temporal and coherence properties accurately, a Maxwell–Bloch approach is required. With the above parameters, we estimate the peak brilliance of the XRL to be  $\sim 4 \times 10^{29}$  photons  $\text{s}^{-1}$  mrad $^{-2}$  mm $^{-2}$  within a relative spectral bandwidth of 0.1%. By comparison, the LCLS has a brilliance of  $\sim 3 \times 10^{31}$  at a photon energy of 1 keV (ref. 8) and can be operated to produce pulses with durations of less than or equal to 10 fs. Considering the absolute bandwidth, the XRL has a spectral brightness only a factor of 30 smaller than that of the LCLS. Notably, the present inner-shell XRL is the shortest-wavelength atomic XRL demonstrated so far and its peak brilliance is greater by two to three orders of magnitude than those of laser-heated XUV plasma lasers<sup>30</sup>.

The XRL photo-ionization scheme can be extended in several ways. The transverse coherence and the brilliance could be increased by lowering the gas density, thereby lengthening the gain region and reducing angular divergence. The output energy of the XRL could be increased significantly by a modest increase in the XFEL energy, as indicated by the theoretical curve in Fig. 3. By increasing the photon energy of the XFEL above the K edges of higher charge states, it should become possible to use hydrogen and helium-like neon as lasing ions<sup>13</sup>. This would result in lines of higher energies and of even narrower bandwidth ( $\Delta\omega/\omega \approx 10^{-6}$ ), owing to the extended lifetime of the

upper state. An increase in the photon flux by a factor of ten and longer pulse durations, in the range of 150–200 fs, would be required to access these lines. The XRL photo-ionization scheme can be transferred to other elements and, thereby, to shorter or longer wavelengths. Lasing on a  $K\alpha$  transition seems to be most promising for elements with atomic number  $Z \leq 20$  (refs 14,25). According to a simplified gain model, the gain-length product scales like  $GL \propto I\lambda^{2.2}$  as wavelength ( $\lambda$ ) decreases (where  $I$  denotes the pump intensity). A numerical study published before XFELs were available showed that lasing in the  $K\alpha$  transition in solid sulphur at 2.37 keV could be established with X-ray pulses nowadays achievable with XFELs<sup>25</sup>. To achieve a gain-length product comparable to that of neon, an increase in the pump intensity by a factor of approximately ten is necessary, which could be achieved by tighter focusing. Another extension is to consider resonant excitation as a pumping mechanism<sup>18</sup>. This scheme, which is based on amplification of self-stimulated X-ray Raman scattering, has the potential of creating phase correlated two-colour X-ray/vacuum-ultraviolet sources suitable for coherent pump–probe applications.

The demonstrated XRL scheme enhances the capability of present-day XFEL sources. By contrast with the SASE XFELs, the atomic XRL is expected to be longitudinally coherent and has a stable wavelength centroid, that is, a highly reproducible spectrum and a much narrower bandwidth. These advantages could be exploited in applications of photoelectron spectroscopy or inelastic X-ray scattering. Moreover, the scheme directly provides a synchronized, that is, time-jitter free, two-colour source in the X-ray regime. Both the transmitted XFEL radiation and the atomic XRL radiation have of the order of  $10^9$ – $10^{10}$  photons per pulse and ultrashort pulse durations of 40 and 5 fs, respectively. The photon energy of the XFEL in this two-colour source is tunable, as long as the photon energy is greater than the K-edge energy of the gain medium. This scheme hence opens the way to two-colour pump–probe studies in the X-ray regime. Intriguing new directions realizable with this kind of source would for example be stimulated inelastic X-ray scattering for applications in solid-state and surface physics or time-resolved molecular spectroscopy by stimulated X-ray Raman scattering<sup>19</sup>.

## METHODS SUMMARY

LCLS X-ray pulses with  $\sim 960$ -eV photon energy were focused to an estimated focus spot of  $\sim 1$ – $2 \mu\text{m}$  radius in a gas cell of 1.4-cm length filled with neon at a pressure of 500 torr. The XFEL pulse energy was varied with a gas attenuator situated upstream and monitored by two upstream pulse-energy detectors. A flat-field grating spectrometer was positioned 4 m downstream of the gas cell to record the spectra of both the transmitted XFEL pump and the XRL line. The spectra were recorded with a conventional 20- $\mu\text{m}$ -pixel back-illuminated X-ray CCD camera. The resolution of the spectrometer is  $\sim 2$  eV at 1-keV photon energy. A triggered shutter allowed for both single-shot and integrated ten-shot measurements, at a repetition rate of the LCLS between 10 and 60 Hz. To estimate the signal and gain parameters of the XRL, we performed self-consistent gain calculations. The model is based on a set of atomic rate equations, determining the populations of a total of 63 configuration states of neon during interaction with an X-ray pulse, coupled to equations describing the propagation, absorption and amplification of the X-ray flux in a simplified one-dimensional geometry. The processes taken into account are photo-ionization of the valence and core shells, Auger decay, spontaneous and stimulated radiative decay, and absorption. We consider the forward-propagating X-ray flux at two discrete energies and assume a dispersion-free medium. Calculations for small signal gain were performed for a stochastic ensemble of SASE pulses, created by a Monte Carlo method. For comparison with the ten-shot data, we assumed flat-top pulses, representing the average temporal structure of the SASE ensemble.

Received 28 August; accepted 15 November 2011.

- Duguay, M. A. & Rentzepis, G. P. Some approaches to vacuum UV and X-ray lasers. *Appl. Phys. Lett.* **10**, 350–352 (1967).
- Matthews, D. L. *et al.* Demonstration of a soft X-ray amplifier. *Phys. Rev. Lett.* **54**, 110–113 (1985).
- Suckewer, S. Skinner, S. Milchberg, C. H., Keane, C. & Voorhees, D. Amplification of stimulated soft X-ray emission in a confined plasma column. *Phys. Rev. Lett.* **55**, 1753–1756 (1985).

4. Elton, R. C. *X-ray lasers* (Academic, 1990).
5. Rocca, J. J. Table-top soft X-ray lasers. *Rev. Sci. Instrum.* **70**, 3799–3827 (1999).
6. Daido, H. Review of soft X-ray laser researches and developments. *Rep. Prog. Phys.* **65**, 1513–1576 (2002).
7. Suckewer, S. & Jaegle, P. X-ray lasers: past, present, future. *Laser Phys. Lett.* **6**, 411–436 (2009).
8. Emma, P. *et al.* First lasing and operation of an ångström-wavelength free-electron laser. *Nature Photon.* **4**, 641–647 (2010).
9. Ackermann, W. *et al.* Operation of a free-electron laser from the extreme ultraviolet to the water window. *Nature Photon.* **1**, 336–342 (2007).
10. Pile, D. X-rays: first light from SACLA. *Nature Photon.* **5**, 456 (2011).
11. Lan, K. Fill, E. & Meyer-ter-Vehn, J. Photopumping of XUV lasers by XFEL radiation. *Laser Part. Beams* **22**, 261–266 (2004).
12. Zhao, J. Dong, Q. L., Wang, S. J., Zhang, L. & Zhang, J. X-ray lasers from inner-shell transitions pumped by the free-electron laser. *Opt. Express* **16**, 3546–3559 (2008).
13. Rohringer, N. & London, R. A. Atomic inner-shell X-ray laser pumped by an X-ray free-electron laser. *Phys. Rev. A* **80**, 013809 (2009).
14. Kapteyn, H. C. Photoionisation-pumped X-ray lasers using ultrashort-pulse excitation. *Appl. Opt.* **31**, 4931–4939 (1992).
15. Rohringer, N. & Santra, R. X-ray nonlinear optical processes using a self-amplified spontaneous emission free-electron laser. *Phys. Rev. A* **76**, 033416 (2007).
16. Kanter, E. P. *et al.* Unveiling and driving hidden resonances with high-fluence, high-intensity X-ray pulses. *Phys. Rev. Lett.* **107**, 233001 (2011).
17. Doumy, G. *et al.* Nonlinear atomic response to intense ultrashort X-rays. *Phys. Rev. Lett.* **106**, 083002 (2011).
18. Sun, Y.-P., Liu, J.-C., Wang, C.-K. & Gel'mukhanov, F. Propagation of a strong X-ray pulse: pulse compression, stimulated Raman scattering, amplified spontaneous emission, lasing without inversion, and four-wave mixing. *Phys. Rev. A* **81**, 013812 (2010).
19. Schweigert, I. V. & Mukamel, S. Probing valence electronic wave-packet dynamics by all X-ray stimulated Raman spectroscopy: a simulation study. *Phys. Rev. A* **76**, 012504 (2007).
20. Tanaka, S. & Mukamel, S. Coherent X-ray Raman spectroscopy: a nonlinear local probe for electronic excitations. *Phys. Rev. Lett.* **89**, 043001 (2002).
21. Mukamel, S. Multiple core-hole coherence in X-ray four-wave-mixing spectroscopies. *Phys. Rev. B* **72**, 235110 (2005).
22. Vartanyants, I. A. *et al.* Coherence properties of individual femtosecond pulses of an X-ray free-electron laser. *Phys. Rev. Lett.* **107**, 144801 (2011).
23. Silfvast, W. T., Macklin, J. J. & Wood, O. R. II. High-gain inner-shell photoionisation laser in Cd vapor pumped by soft-X-ray radiation from a laser-produced plasma source. *Opt. Lett.* **8**, 551–553 (1983).
24. Kapteyn, H. C., Lee, R. W. & Falcone, R. W. Observation of short-wavelength laser pumped by Auger decay. *Phys. Rev. Lett.* **57**, 2939–2942 (1986).
25. Axelrod, T. S. Inner-shell photoionisation-pumped X-ray lasers. Sulfur. *Phys. Rev. A* **13**, 376–382 (1976).
26. Eder, D. C. *et al.* Tabletop X-ray lasers. *Phys. Plasmas* **1**, 1744–1752 (1994).
27. Strobel, G. L. *et al.* Innershell photoionized X-ray laser schemes. *Proc. SPIE* **1860**, 157–166 (1993).
28. Young, L. *et al.* Femtosecond electronic response of atoms to ultra-intense X-rays. *Nature* **466**, 56–61 (2010).
29. Hopf, F. A. & Meystre, P. Quantum theory of a swept-gain laser amplifier. *Phys. Rev. A* **12**, 2534–2548 (1975).
30. Rus, B. *et al.* Multimillijoule, highly coherent X-ray laser at 21 nm operating in deep saturation through double-pass amplification. *Phys. Rev. A* **66**, 063806 (2002).

**Supplementary Information** is linked to the online version of the paper at [www.nature.com/nature](http://www.nature.com/nature).

**Acknowledgements** This work was performed under the auspices of the US Department of Energy by Lawrence Livermore National Laboratory (LLNL; DE-AC52-07NA27344) and was supported by LLNL's LDRD programme, 09-LW-044. Portions of this research were carried out at the Linac Coherent Light Source, a national user facility operated by Stanford University on behalf of the US Department of Energy, Office of Basic Energy Sciences. J.J.R., M.P. and D.R. were supported by the US Department of Energy Basic Energy Sciences AMOS Program. We thank M. J. Pivovarov and K. A. van Bibber for their encouragement and support for this project; R. W. Lee, T. Ditmire, L. Young, R. Falcone and S. Le Pape for discussions of the experimental design; J.-C. Castagna, C.-M. Tsai, S. Schorb, M. L. Swiggers and M. Messerschmidt for their assistance with the experiment; M. J. Bogan for the loan of the X-ray CCD camera and A. Barty for the design of Fig. 1. We also acknowledge support of the LCLS software engineers for the control and data acquisition. We are indebted to the LCLS operating team for their support during beam time in achieving the necessary pulse energies for this experiment.

**Author Contributions** N.R. and R.A.L. had the idea for the experiment, which was designed with J.J.R., J.D. and J.D.B. N.R. developed theory and models of the data. J.D.B. and C.B. were responsible for the AMO beamline at LCLS. R.H. designed the neon gas cell. D.R. and M.P. calibrated and installed the X-ray spectrograph. D.R., M.P., J.D.B., C.B., J.D., F.A., N.R., J.J.R. and R.A.L. carried out the experiment. S.P.H.-R. and R.A.L. performed hole-drilling tests on the gas-cell window materials. A.G. helped in the set-up of the experiment. J.D., R.A.L. and N.R. designed the filters. N.R., D.R. and R.A.L. analysed and interpreted the data. R.A.L. estimated the gain and gain-length product. N.R. wrote the paper with contributions from R.A.L., J.D., D.R. and J.J.R.

**Author Information** Reprints and permissions information is available at [www.nature.com/reprints](http://www.nature.com/reprints). The authors declare no competing financial interests. Readers are welcome to comment on the online version of this article at [www.nature.com/nature](http://www.nature.com/nature). Correspondence and requests for materials should be addressed to N.R. ([nina.rohringer@asg.mpg.de](mailto:nina.rohringer@asg.mpg.de)).